THE PUBLISHING HOUSE
OF THE ROMANIAN ACADEMY

PROCEEDINGS OF THE ROMANIAN ACADEMY, Series A,
Volume 20, Number 4/2019, pp. 383–391

ON THE SINGULARITY-FREE WORKSPACE OF A PARALLEL ROBOT FOR LOWER-LIMB REHABILITATION

Bogdan GHERMAN[1], Iosif BIRLESCU[1], Nicolae PLITEA[1], Giuseppe CARBONE[1,2], Daniela TARNITA[3], Doina PISLA[1]

[1] Technical University of Cluj-Napoca, CESTER, B-dul Muncii 103-105, 400641 Cluj-Napoca, Romania
[2] DIMEG, University of Calabria, Via Bucci, Cubo 46C, 87036 Rende (Cs), Italy
[3] University of Craiova, Alexandru Ioan Cuza 13, Craiova 200585
Corresponding authors: Doina PISLA, E-mail: doina.pisla@mep.utcluj.ro
Daniela TARNITA, E-mail: tarnita.daniela@gmail.com

Abstract. The paper presents the workspace determination of RECOVER, a parallel robotic system designed for lower limb rehabilitation. The kinematic model was formulated to achieve a direct correlation between the active joints of the robot and the anatomic joint angles. The singularities of the robotic system are analysed with respect to the medical task and anatomical constraints, showing that the robot task orientated workspace is singularity-free. Experimentally measured data regarding the gait cycle are compared with numerical simulations, showing the feasibility of the RECOVER parallel robotic system for gait rehabilitation.

Key words: parallel robot, medical rehabilitation, singularity, workspace.

1. INTRODUCTION

Stroke represents the second leading cause of death and a major cause of disability all over the world, whose incidence is increasing with the age of the population. In the European Union, approximately 1.1 million inhabitants suffer a stroke each year and by 2025 the projections show an increase to 1.5 million, while the vast majority remain with permanent disabilities at various degrees [1]. The main methods of post-stroke rehabilitation are physical therapy and occupational therapy [2], which involves the practice of repetitive motions by a disabled patient, targeting the affected group of muscles and being usually performed under strict supervision of qualified medical staff. Since robotic devices deliver advantages like: higher intensity exercises, the possibility to work with more patients in the same amount of time and a precise analysis of the patient rehabilitation progress for a highly objective evaluation [3], a strong need for such devices becomes obvious. Most of the robotic systems developed for lower limb rehabilitation are exoskeletons [4-6], able to sustain the whole body weight. Other robotic systems [7–11] are designed to perform certain guided movements of the lower limbs to obtain a higher efficiency during therapeutic exercises, to improve mobility of the patient's joints and to get a better motion coordination and a certain strengthening of the lower limb muscles. There are systems that target only the ankle rehabilitation, and literature indicates that parallel architectures are good candidates for these types of robots, some of these using redundant actuators to increase the stiffness [12–13]. A novel robotic system RECOVER designed for lower limb rehabilitation was previously introduced and analysed [17,18]. Its' kinematics were derived using a classical approach where the motion of a mobile platform was studied. However, the kinematic model was not sufficient to describe the motion of the anatomic joints and more equations were needed.

The current paper aims to illustrate the singularity-free workspace of the RECOVER parallel robot, based on a kinematic model which yields constraint equations that directly describe the anatomic joints motion relative to the active joints of the robot. Section 2 derives the kinematics while Section 3 describes the singularities. The singularity free workspace is generated in Section 4, and numerical simulations are shown. A discussion is presented in Section 5, and the conclusions are drawn in Section 6.

2. KINEMATICS

The kinematic model presented in the paper (in contrast with [17, 18]) creates direct relations between the RECOVER active joints and angles of the anatomic joints of the lower limb (hip, knee, and ankle). The parallel robotic system for post stroke rehabilitation of the lower limb is designed for bedridden patients, and it consists of two serialized parallel robotic modules (see Fig. 1): the ***Hip-Knee module*** with 2 DOF designed for hip and knee flexion/extension and the ***Ankle module*** with 2 DOF designed for ankle flexion/extension and inversion/eversion. The relations between active joints and specific angles are determined by eliminating the coordinates of the mobile platform together with the free motion parameters. The kinematic formulation is based on the Denavit-Hartenbeg convention based on homogeneous transformation matrices.

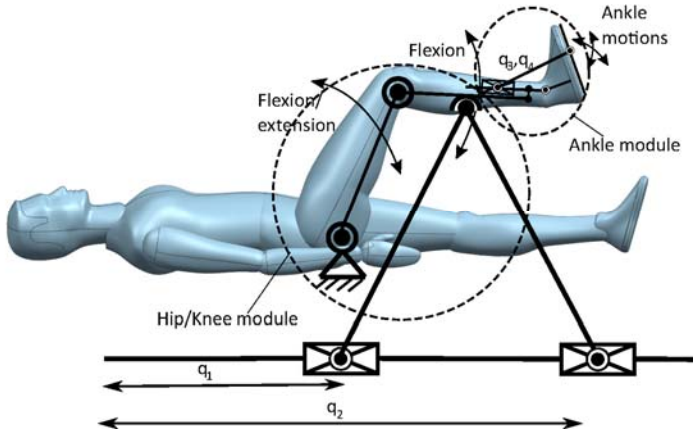

Fig. 1 – RECOVER parallel robot conceptual design.

The kinematic chains of the ***Hip-Knee module*** [17] (Fig. 2a) are defined as follows: K_{chain0} is a RR linkage, composed of the R_h, R_k revolute joints (free rotation motions) and the L_f, L_t links; K_{chain1} and K_{chain2} are two identical PRR kinematic chains, actuated by q_1 and q_2 respectively. K_{chain1} contains the revolute joint R_1 and the link l_1 (rotating around R_1 rotation axis), while K_{chain2} contains the revolute joint R_2 and the link l_2 (rotating around R_2). Both K_{chain1} and K_{chain2} intersect in the rotation axis of the revolute joint R_3 (in the origin of the moving frame $O'X'Y'Z'$). The kinematic chains of the ***Ankle module*** (Fig. 2b) are defined as: A_{chain0} is an RR linkage with the revolute joints (R_{a1}, R_{a2} as free rotations) having orthogonal axes (which intersect in the origin of both fixed and moving coordinate frames). The chain supports the patients' sole in a way that the ankle rotation axes should be aligned with the R_{a1}, R_{a2} axes. The distance l_s should be adjustable to account for anthropomorphic variations; A_{chain1} and A_{chain2} are two identical PSS input chains, symmetrically assembled with respect to the X^*Y^* plane. A_{chain1} starts at a distance L_0 on Z^* direction ($-L_0$ for the A_{chain2}), is actuated by q_3 on $-X^*$ direction (q_4 for A_{chain2}), and has the link l_{a1} between the two spherical joints S_1, S_2 (l_{a2} is placed between S_3 and S_4 for A_{chain2}).

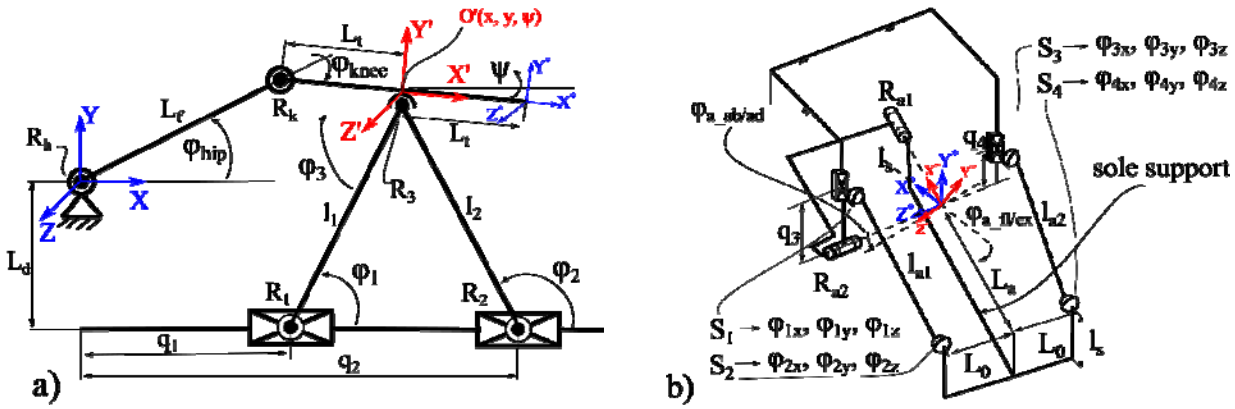

Fig. 2 – Kinematic schemes for: a) the Hip-Knee module; b) the Ankle module.

The DH matrices for the ***Hip-Knee module*** kinematic chains are:

$$K_{chain0} = T_D \cdot R_Z(\varphi_{hip}) \cdot T_X(L_f) \cdot R_Z(\varphi_{knee}) \cdot T_X(L_t) \tag{1}$$

$$K_{chain1,2} = T_{D1,2} \cdot T_X(q_{1,2}) \cdot R_Z(\varphi_{1,2}) \cdot T_X(l_{1,2}) \cdot R_Z(\varphi_3) \tag{2}$$

Since the chains must intersect in the origin of the moving frame $O'X'Y'Z'$, $K_{chain0} - K_{chain1} = 0$ is true. It follows that $K_{chain0}[1,2] = K_{chain1}[1,2]$, $K_{chain0}[1,3] = K_{chain1}[1,3]$, ratios that define two constraint equations for the ***Hip-Knee module*** using the geometric substitutions for the unknown rotations (with $l_{a1}=l_{a2}$):

$$\begin{cases} h_1 : L_f \cdot \cos(\varphi_{hip}) + L_t \cdot \cos(\varphi_{hip} - \varphi_{knee}) - (q_1 + \cos(\varphi_1) l_1) \\ h_2 : L_f \cdot \sin(\varphi_{hip}) + L_t \cdot \sin(\varphi_{hip} - \varphi_{knee}) - (-L_d + \sin(\varphi_1) \cdot l_1) \end{cases}$$

$$\text{with: } \begin{cases} \cos(\varphi_1) \cdot l_1 = \dfrac{q_2 - q_1}{2} \\ \sin(\varphi_1) \cdot l_1 = \sqrt{l_1^2 - \left(\dfrac{q_2 - q_1}{2}\right)^2} \end{cases} \tag{3}$$

Referring to Fig. 1b, the DH matrices for the ***Ankle module*** kinematic chains are:

$$A_{chain0} = T_D \cdot R_Z(\varphi_{a\_fl/ex}) \cdot R_Y \cdot (\varphi_{a\_ev/iv}) \tag{4}$$

$$\begin{aligned} A_{chain1(2)} = \quad & T_{D1(2)} \cdot T_X(-q_{3(4)}) \cdot R_Z(\varphi_{1(3),z}) \cdot R_Y(\varphi_{1(3),y}) \cdot R_X(\varphi_{1(3),x}) \cdot \\ & T_X(l_{a1(2)}) \cdot R_Z(\varphi_{2(4),z}) \cdot R_Y(\varphi_{2(4),y}) \cdot R_X(\varphi_{2(4),x}) \cdot T_X(-L_a) \cdot T_Z(\mp L_0). \end{aligned} \tag{5}$$

where the following relation is true (since all chains meet in the same point) $A_{con} : A_{chain1} + A_{chain2} - 2A_{chain0} = 0$, with A_{con} being the transformation matrix for the ***Ankle module***. The terms $A_{con}[2,2]$ and $A_{con}[2,3]$ are sufficient to define the two constraint equations for the ***Ankle module*** (Eq. 6), where the following notations are used: $c_{1(3),z}$ are the cosines of the rotation angles around the local rotation axis Z for the spherical joints S_1 and S_3 respectively; $s_{1(3),y}$ are the sines of the rotation angles of the local rotation axis Y of the spherical joints S_1 and S_3 respectively, and so on. The notation remains consistent for all rotation parameters introduced by all 4 spherical joints (see Fig. 1b). The notations for the rotation parameters for the anatomic joints (e.g. $\cos(\varphi_{a\_ev/inv})$) remain unchanged. Moreover, a series of geometric substitutions are applied (Eq. 7) to eliminate the unknown rotation parameters and obtain constraint equations depending only on the active joint parameters, ankle joint angles, and constant geometric values for the mechanism links.

$$\begin{cases} h_3 : (1 + (c_{2,z} - 1)c_{1,y}^2)c_{1,z} - s_{1,z}c_{1,y}s_{2,z} + (1 + (c_{4,z} - 1)c_{3,y}^2) - s_{3,z}c_{3,y}s_{4,z} - 2\cos(\varphi_{a\_fl/ex})\cos(\varphi_{a\_ev/iv}) \\ h_4 : (c_{1,z}c_{1,y}s_{2,z} - s_{1,z}c_{2,z}) + (c_{3,z}c_{3,y}s_{4,z} - s_{3,z}c_{4,z}) + 2\sin(\varphi_{a\_fl/ex}) \end{cases} \tag{6}$$

$$\begin{cases} c_{1(3),z} = \dfrac{q_{3(4)}^2 - L_a^2 + l_{a1(a2)}^2}{2q_{3(4)}l_{a1(a2)}}; \quad c_{2(4),z} = \dfrac{-q_{3(4)}^2 + L_a^2 + l_{a1(a2)}^2}{2L_a l_{a1(a2)}}; \quad s_{1(3),y} = \dfrac{2A_{1(2)}}{q_{3(4)}l_{a1(a2)}}; \quad s_{2(4),y} = \dfrac{2A_{1(2)}}{L_a l_{a1(a2)}}; \\ A_{1(2)} = \sqrt{s_{p1(2)}(s_{p1(2)} - q_{3(4)})(s_{p1(2)} - l_{a1(a2)})(s_{p1(2)} - L_a)}; \quad s_{p1(2)} = \dfrac{1}{2}(q_{3(4)} + l_{a1(a2)} + L_a); \\ c_{1(3),y} = \dfrac{q_3\cos(\varphi_{a\_fle/ex}) - L_a\sin(\varphi_{a\_ev/iv})}{q_3\cos(\varphi_{a\_fl/ex})}; \quad s_{1(3),y} = \dfrac{L_a - L_a\cos(\varphi_{a\_ev/iv})}{q_3\cos(\varphi_{a\_fl/ex})}; \\ c_{1(2),x} = 1; \quad s_{1(2),x} = 0; \quad c_{3(4),x} = 1, \quad s_{3(4),x} = 0, \quad c_{2(4),y} = -c_{1(3),y}; \quad s_{2(4),y} = -s_{1(3),y}. \end{cases} \tag{7}$$

3. SINGULARITIES ANALYSIS

The singularities for the RECOVER parallel robotic modules are determined by the vanishing condition of the determinants of the Jacobi matrices (where J_a, J_q refer to the ***Hip-Knee module***, and J_a^*, J_q^* to the ***Ankle module*** respectively):

$$J_a=\left[\frac{\partial(h_1,h_2)}{\partial(\varphi_{hip},\varphi_{knee})}\right];\quad J_q=\left[\frac{\partial(h_1,h_2)}{\partial(q_1,q_2)}\right];\quad J_a^*=\left[\frac{\partial(h_3,h_4)}{\partial(\varphi_{a\_fl/ex},\varphi_{a\_ev/iv})}\right];\quad J_q^*=\left[\frac{\partial(h_3,h_4)}{\partial(q_3,q_4)}\right]. \tag{8}$$

For the ***Hip-Knee module*** the determinants have the explicit form:

$$\det(J_a)=L_f L_t\sin(\varphi_{knee});\quad \det(J_q)=\frac{1}{2}(q_1-q_2)\frac{1}{\sqrt{4l_1^2-q_1^2+2q_1q_2-q_2^2}}, \tag{9}$$

where $\det(J_a)$ (Eq.9) is a product of three factors, with the first 2 being geometric parameters (which will never be 0). The last factor becomes 0 for (φ_{knee} = 0, 180°), and defines the **1st *Hip-Knee module singularity*** when the kinematic chain A_{chain0} is fully stretched or folded. This condition should be considered in the control (or in the mechanical design) to allow the safe exploitation of the system during the rehabilitation exercises, using techniques like in [19] or even a dynamic control as in [20]. The **2nd** and **3rd *Hip-Knee module singularity*** ($\det(J_q)$ = 0, see Eq.9) configurations occurs when the two links l_1, l_2 are coincidental ($q_1=q_2$) or aligned ($q_{1,2}=q_{2,1}\pm 2l_1$) respectively. These singularities should be avoided either in the control system or in the mechanical design (by imposing or limiting the stroke limits of the active joints).

For the ***Ankle module*** the determinants are:

$$\det(J_a^*)=\frac{1}{2}\frac{1}{l_{a1}^2q_3^2L_aq_4}f(\varphi_{a\_fl/ex},\varphi_{a\_ab/ad},q_3,q_4,l_{a1},L_a,L_0) \tag{10}$$

$$\begin{aligned}&\det(J_q^*)=\frac{1}{8}F_2F_3F_4F_5;\quad F_2=\frac{1}{q_3^4l_{a1}^4L_a^2q_4^3};\quad F_3=f(\varphi_{a\_fl/ex},q_3,q_4,l_{a1},L_a,L_0)\\ &F_4=\frac{1}{\sqrt{-(q_3+l_{a1}+L_a)(-q_3+l_{a1}+L_a)(q_3-l_{a1}+L_a)(-q_3-l_{a1}+L_a)}}\\ &F_5=\frac{1}{\sqrt{-(q_4+l_{a1}+L_a)(-q_4+l_{a1}+L_a)(q_4-l_{a1}+L_a)(-q_4-l_{a1}+L_a)}}\end{aligned} \tag{11}$$

where $\det(J^*_a)$ (Eq.10) is a product of three factors where the first one is a scalar, so not of interest. The second factor holds geometric information where the links lengths l_{a1} and L_a are not allowed to be zero (which will never be the case). The **1st *Ankle module singularity*** occurs when q_3 or q_4 are zero. By imposing specific link lengths ($l_{a1}\neq L_a$) this singularity is easily avoided. The third factor of $\det(J^*_a)$ (Eq.10) is a function of all the parameters used in the derivation of the constraints (only presented in general form due to its length). The factor was evaluated with numerical values for the geometric parameters $\{l_{a1}=5$, $L_a=4$, $L_0=1\}$ and solved for the angles $\varphi_{a\_ev/iv}$, $\varphi_{a\_fl/ex}$ obtaining a set of 9 solutions (Sol_i $i=1...9$). The first 4 solutions (Sol_i $i=1...4$) have the form $\{\varphi_{a\_ev/iv}=\pm\pi/2$, $\varphi_{a\_fl/ex}=\pm\pi/2\}$. Substituting these solutions back into $\det(J^*_a)$ the determinant vanishes, thus defining the **2nd *Ankle module singularity***, when the eversion/inversion angle is 90° (but the angle is not in the task workspace since it exceeds the natural capabilities of the ankle joint). The next 4 solutions (Sol_i $i=5...8$) have the form $\{\varphi_{a\_ev/iv}=f(q_3,q_4)$, $\varphi_{a\_fl/ex}=0$ or $\pi\}$ where the values 0 or π for $\varphi_{a\_fl/ex}$ describes the mobile platform in vertical position. The **3rd *Ankle module singularity*** occurs when the flexion/extension angle is ±90° (since the 0 angle of the ankle joint is represented by $\varphi_{a\_fl/ex}=\pi/2$ due to the parameterization). But the angle is outside the task workspace. The last solution (Sol_9), revealed a particular configuration where the projection of L_0 and l_{a1} onto the plane Y^*Z^* are aligned. Explicitly, the **4th *Ankle module singularity*** occurs when $(Proj_{Y^*Z^*}(L_0)\times Proj_{Y^*Z^*}(l_{a1})=0)$. Choosing optimal lengths for the geometric parameters for the ***Ankle module*** results in having this singularity near the boundary of the workspace and therefore, outside the task workspace of the module. The

factors of the determinant $\det(J^*_q)$ (Eq. 11) showed the same singularity configurations already determined using the determinant $\det(J^*_a)$ (Eq. 10).

4. WORKSPACE GENERATION

4.1. Design constraints

For a better understanding of the ***medical task constraints***, in order to achieve a successful design of RECOVER, the authors have carried out a gait study using the Optitrack Motion Capture tracking system (Fig. 3). A number of 15 healthy individuals have taken part in the study, which consisted in performing the tracking of 8 highly reflective markers attached to the subject's leg during normal walking, as follows: two markers on the foot (defining the $\boldsymbol{v}_1$ vector), two on the leg (defining $\boldsymbol{v}_2$), two on the thigh (defining $\boldsymbol{v}_3$), and two on the trunk (defining $\boldsymbol{v}_4$). Fig. 4 presents the time history diagram of the measured values for a male with a height of 180 cm (very similar results have been obtained for all others 14 subjects) for the angles formed between these vectors (after de-noising with FFT), namely: the angle between $\boldsymbol{v}_3$ and $\boldsymbol{v}_4$ (which stands for the hip flexion/extension), the angle between $\boldsymbol{v}_2$ and $\boldsymbol{v}_3$ (which stands for the knee flexion) and the angle between $\boldsymbol{v}_1$ and $\boldsymbol{v}_2$ (which stands for the plantar flexion/dorsiflexion). In addition, Fig. 4 presents the velocities recorded for each angle during the same walking measurements (values that the robot must comply with to ensure the efficiency of the rehabilitation procedures).

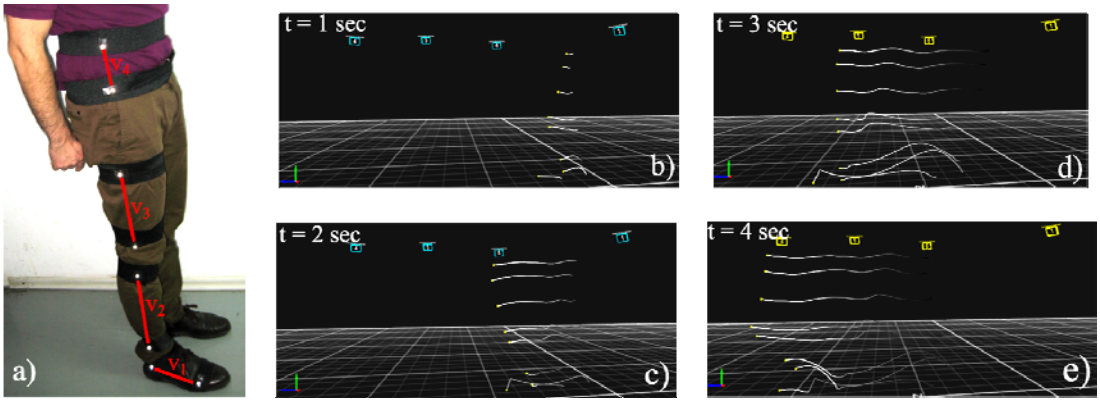

Fig. 3 – Optitrack experimental setup: markers' position on the subject's body (a); markers within motive software (b-d).

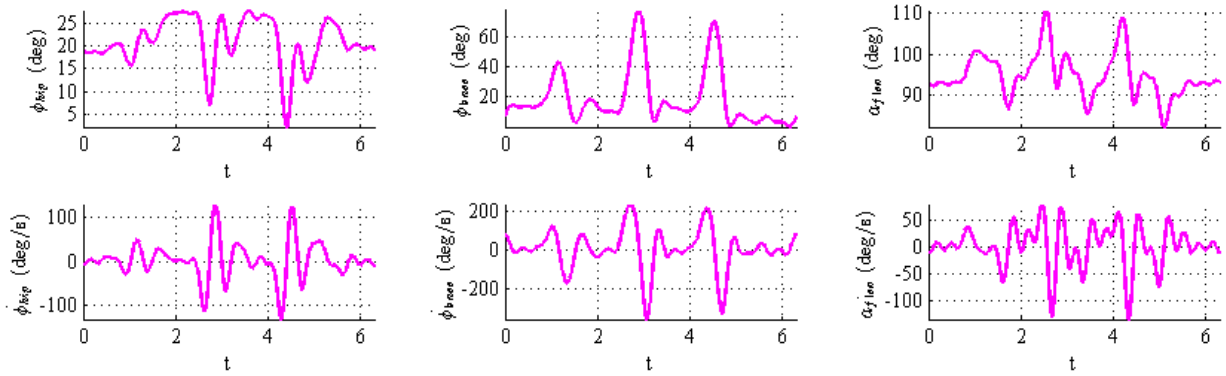

Fig. 4 – The time history diagram of the angles and velocities from the Optitrack measurements.

To determine the links dimensions of RECOVER, the ***anthropomorphic constraints*** have been considered. Since the ***Hip-Knee module*** must comply with anthropometric variations (using variable values for the L_f, and L_t), in the mechanism design the upper portion of the normal distribution among patient limb segment lengths is considered, as in [14]. The initial experimental values of L_f and L_t are chosen based on a human

male of 1900 mm height with approx. **465 mm** upper leg maximum length, and **460 mm** lower leg maximum length (which is $2L_t$ – see Fig. 2a) [14], but, as Fig. 8 later shows, RECOVER should and does also fit a 150cm height subject. The lengths of the other components were determined based on the maximum and minimum values for the anatomic joint angles, as in [14]. Choosing $L_d = \mathbf{400\ mm}$ (appropriate distance accounting the bed height), and imposing $(q_1 - q_2) > \mathbf{200\ mm}$ (to avoid collisions), the lengths (l_1, l_2) and the active joint strokes values were determined using the constraint equations (Eq. 3) were the joint angle values were substituted in, and the equations were solved for the link parameters, and the active joints respectively. The computed numerical values are: $l_1, l_2 = \mathbf{960\ mm}$, $q_2 < \mathbf{1680\ mm}$, $q_1 > -\mathbf{930\ mm}$ ($q_1 > q_2$).

In the case of the Ankle module there is no need of adjusting the L_a, l_a, L_0 lengths, as long as the ankle joint is correctly aligned with the revolute joint axes R_{a1}, R_{a2}. The only anthropometric adjustment is the distance between the patient's sole and the intersection point of the R_{a1} and R_{a2} rotation axes (l_s). The chosen lengths for the links are: $L_a = \mathbf{140\ mm}$, $L_0 = \mathbf{35\ mm}$, $l_a = \mathbf{175\ mm}$. For these values, all the singularities are at the edge of the workspace, creating a singularity free task oriented workspace.

4.2. Singularity-free workspace generation

The workspace of the ***Hip-Knee module*** is illustrated in Fig. 5 and it has been obtained using the numerical values discussed in Section 4.1 $\{L_f = 470,\ L_t = 270,\ l_1 = 960,\ L_d = 400\}$. The workspace is computed from two implicit surfaces (for both the parametrizations of the free chain and the input chains (h_1, h_2 – see Eq. 3) where the surface describing the constraints of the free chain (the paraboloid M_2 – Fig. 5c) is projected onto the surface that describes the input chains (the slanted cylinder M_1 – Fig. 5b).

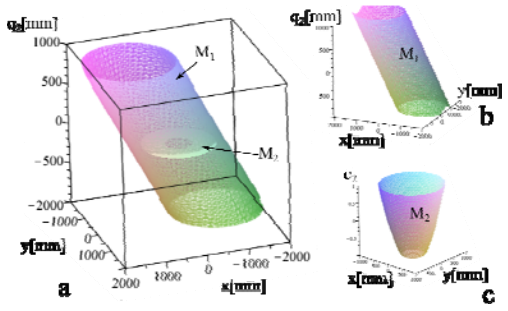

Fig. 5 – Surfaces for the Hip-Knee module workspace.

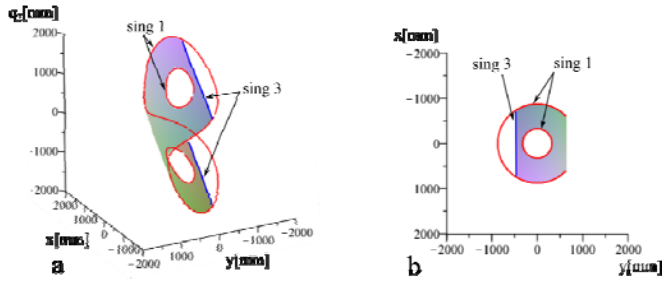

Fig. 6 – Singularity free workspace of the Hip-Knee module.

The implicit surfaces were computed using Groebner bases techniques [21,22]. The implicit representation of parameterization defined by a finite set of polynomials may be computed using a Groebner base by eliminating parameters [22]. To allow the base computation of h_1 (Eq. 3) the square root is eliminated by algebraic manipulation and squaring the equation. Moreover, for h_2 (Eq. 3) the normalizing conditions are added in the computation: $s_1^2 + c_1^2 - 1 = 0$, $s_2^2 + c_2^2 - 1 = 0$. The active joint q_1 is eliminated from the input chains parameterization and s_1, c_1 are eliminated from the free chain parameterization. Fig. 6 illustrates the singularity free workspace (in isometric view Fig. 6a, and side view Fig. 6b), where: *sing*1 is the **1st *Hip-Knee module singularity***, *sing* 2 is the **3rd *Hip-Knee module singularity***; the **2nd *Hip-Knee module singularity*** is not achievable within the workspace due to the constraint $(q_1 - q_2) > 200$.

Fig. 7 illustrates slices of the ***Ankle module*** workspace corresponding to the limits of the flexion/extension motion, and the limits of the eversion/inversion. The slices were determined after the computation of the workspace (using Eq. 6) with the trigonometric functions substituted with algebraic terms: $\cos(\varphi_{a\_ab/ad}) = c_{\varphi 1}$, $\sin(\varphi_{a\_ab/ad}) = s_{\varphi 1}$, $\cos(\varphi_{a\_fl/ex}) = c_{\varphi 2}$, $\sin(\varphi_{a\_fl/ex}) = s_{\varphi 2}$. The workspace was computed in two ways. On the one hand, a Groebner base was computed from h_3, h_4 (Eq. 6) using $s_{\varphi 1} > c_{\varphi 1} > s_{\varphi 2} > c_{\varphi 2}$ ordering, thus obtaining an implicit representation that correlates the eversion/inversion with the active joints (at different flexion/extension angles), Fig. 7a. On the other hand, a second Groebner base was computed from h_3, h_4 using $s_{\varphi 2} > c_{\varphi 2} > s_{\varphi 1} > c_{\varphi 1}$ ordering, obtaining an implicit representation that correlates the flexion/extension with the active joints (at different eversion/inversion angle values), Fig. 7b. To generate the workspace the equations were evaluated with $\{L_a = 140,\ L_0 = 35,\ l_{a1(2)} = 175\}$. Moreover, the square root

terms were eliminated through algebraic manipulation (and squaring the equations), and the normalizing conditions ($c^2_{\varphi 1}+s^2_{\varphi 1}-1=0$, $c^2_{\varphi 2}+s^2_{\varphi 2}-1=0$) were added in the computation.

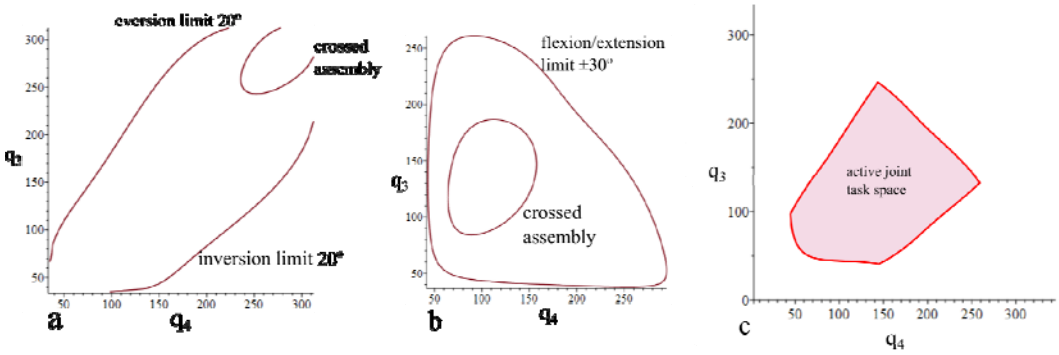

Fig. 7 – Ankle module workspace slices: a) flexion/extension motion; b) eversion/inversion motion; c) active joint task space.

The slices of the surfaces were taken at the values $c_{\varphi 2}=0.94$ (at 20° eversion/inversion limit – Fig. 7a), and $c_{\varphi 1}=0.86$ (for the flexion/extension angle limit of ±30° Fig. 7b). Both curves represent the boundary of the task space. The "egg shaped" curves represent an assembly mode where the l_{a1} and l_{a2} links are crossed and therefore are not of interest. Overlapping the curves envelops an area that describes the active joint "task oriented space" (Fig. 7c) which is singularity free (see Section 3).

4.3. Numerical simulations

Figure 8 presents the results of a simulation describing the active joints (positions, velocities and accelerations) of RECOVER performing the gait exercise with the anatomic joint motions for three patients, having different heights: 150 cm, 180 cm and 190 cm. Fig. 8 proves that RECOVER can be used for the gait training task for a large spectrum of patients' sizes. Different patient's size does not influence the kinematics of the ***Ankle module***, so the q_3-q_4 active joints time history diagram are the same for the three patients. The large variations (and distance) of the active joints are within the active joint stroke limits which together with the workspace analysis shows the feasibility of the RECOVER robotic system for the gait training.

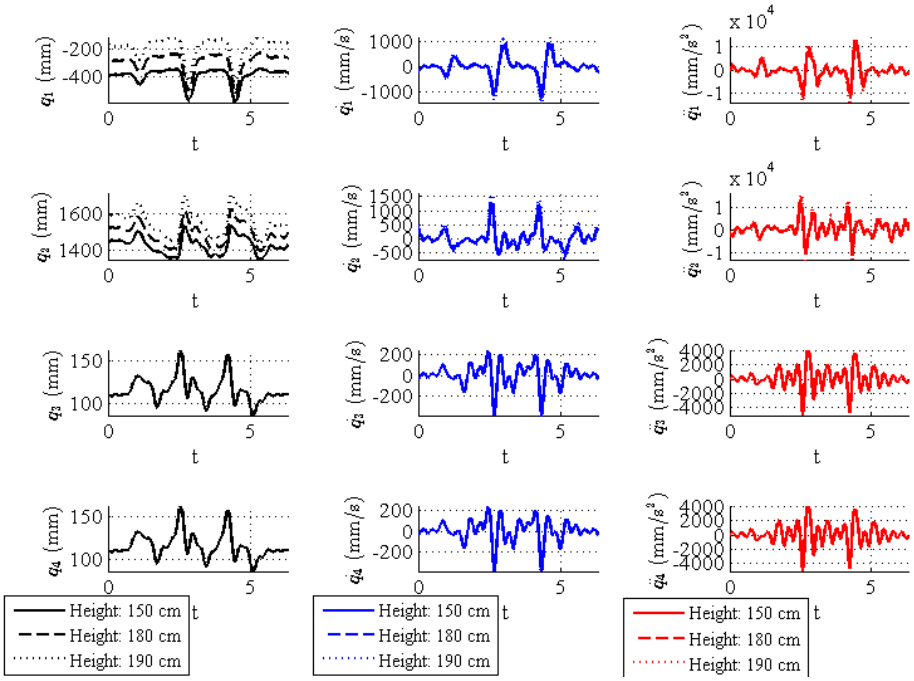

Fig. 8 – Time history diagram of the RECOVER active joints (positions, velocities and accelerations) for the gait cycle.

5. DISCUSSION

In the field of post stroke rehabilitation, often, medical personnel are interested in specific anatomic joints motion capabilities such as amplitude of motion, velocities and accelerations. The mathematical approach used in this paper, makes a direct correlation between these anatomic joint angles and the robot actuators, made possible by the close relation between the human joints and the robot design. Although previous studies on the RECOVER robotic system [17, 18] reveal the same behaviour for the ***Hip-Knee module***, by this approach, the kinematics, singularities and workspace were derived using the direct correspondence between the robot actuators and the human lower limb joints. Since the singularity configurations show up outside the task space (with the one exception where the leg is fully stretched – which must be accounted for) defined by the medical personnel as the limits of each anatomic joint value, the robot proves to be suitable for rehabilitation purposes.

7. CONCLUSIONS

The paper presents the singularity-free workspace of the RECOVER parallel robot for gait rehabilitation, which was computed based on a kinematic model that directly links the active joints of the robot to the anatomic joint angle values. The mechanisms singularities were also described in terms of values of the anatomic joint angles. Using gait data obtained by tracking healthy subjects (together with anthropomorphic data), the gait task was defined and the RECOVER parallel robotic system was simulated performing the task. The simulation showed the feasibility of the RECOVER system for the gait rehabilitation.

ACKNOWLEDGMENTS

The paper presents results from the research activities of the project ID 37_215, MySMIS code 103415 "Innovative approaches regarding the rehabilitation and assistive robotics for healthy ageing" cofinanced by the European Regional Development Fund through the Competitivness Operational Programme 2014-2020, Priority Axis 1, Action 1.1.4, through the financing contract 20/01.09.2016, between the Technical University of Cluj-Napoca and ANCSI as Intermediary Organism in the name and for the Ministry of European Funds.

REFERENCES

1. Y. BEJOT, H. BAILLY, J. DURIER, M. GIROUD, *Epidemiology of stroke in Europe and trends for the 21st century*, Presse Med, **45**, *12*, pp. 391-398, 2016.
2. W. CHEN, R. GAO, *China cardiovascular disease report 2013*, Chinese Circulation Journal, **29**, *7*, pp. 487-491, 2014.
3. S. DEHEM, M. GILLIAUX, T. LEJEUNE, C. DETREMBLEUR, D. GALINSKI, J. SAPIN, M. VANDERWEGEN, G. STOQUART, *Assessment of upper limb spasticity in stroke patients using the robotic device REAplan*, Journal of Rehabilitation Medicine, **49**, *7*, pp. 565-571, 2017.
4. S.A. KOLAKOWSKY-HAYNER, J. CREW, S. MORAN, A. SHAH, *Safety and feasibility of using the Ekso™ bionic exoskeleton to aid ambulation after spinal cord injury*, The Spine Journal, **4**, *3*, 2013.
5. G. ZEILIG, H. WEINGARDEN, M. ZWECKER, I. DUDKIEWICZ, A. BLOCH, A. ESQUENAZI, *Safety and tolerance of the ReWalk™ exoskeleton suit for ambulation by people with complete spinal cord injury: A pilot study*, The Journal of spinal cord medicine, **35**, *2*, pp. 96-101, 2012.
6. B. MICHAUD, Y. CHERNI, M. BEGON, G. GIRARDIN-VIGNOLA, P. ROUSSEL, *A serious game for gait rehabilitation with the Lokomat*, 2017 International Conference on Virtual Rehabilitation (ICVR), Montreal.
7. M. BOURI, Y. STAUFFER, C. SCHMITT, Y. ALLEMAND, S. GNEMMI, R. CLAVEL, P. METRAILLER, R. BRODARD, *The walktrainer: a robotic system for walking rehabilitation*, Proceedings of the IEEE International Conference on Robotics and Biomimetics, Kunming, China, 2006, pp. 1616–1621.
8. M. BOURI, B. LE GALL, R. CLAVEL, *A new concept of parallel robot for rehabilitation and fitness: the Lambda*, Proceedings of the IEEE International Conference on Robotics and Biomimetics, Guilin, China, 2009, pp. 2503–2508.
9. S. SARGSYAN, V. ARAKELYAN, S. BRIOT, *Robotic rehabilitation devices of human extremities: design concepts and functional particularities*, ASME 2012 11th Biennial Conference on Engineering Systems Design and Analysis, Nantes, France, 2012, pp. 245-254.

10. K. KONG, M. TOMIZUKA, *Design of a rehabilitation device based on a mechanical link system,* Journal of Mechanisms Robotics, **4**, *3*, p. 035001, 2012.
11. C. VAIDA, I. BIRLESCU, A. PISLA, G. CARBONE, N. PLITEA, I. ULINICI, B. GHERMAN, F. PUSKAS, P. TUCAN, D. PISLA, *RAISE – An innovative parallel robotic system for lower limb rehabilitation*, New Trends in Medical and Service Robotics, Mechanisms and Machine Science, **65**, pp. 293-302, 2019.
12. J.A. SAGLIA, N.G. TSAGARAKIS, J.S. DAI, D.G. CALDWELL, *A high-performance redundantly actuated parallel mechanism for ankle rehabilitation*, International Journal of Robotics Research, **28**, *9*, pp. 1216-1227, 2009.
13. C. WANG, Y. FANG, S. GUO, Y. CHEN, *Design and kinematical performance analysis of a 3-RUS/RRR redundantly actuated parallel mechanism for ankle rehabilitation*, J. Mechanisms Robotics, **5**, *4*, p. 041003, 2012.
14. R. DRILLS, R. CONTINI, M. BLUENSTEIN, *Body segment parameters – A survey of measurement techniques*, Artificial Limbs, **8**, *1*, pp. 44-66, 1964.
15. S. PLAGENHOEF, F. GAYNOR EVANS, T. ABDELNOUR, *Anatomical data for analyzing human motion*, J. Research Quarterly for Exercise and Sport, **52**, *2*, pp. 169-178, 1983.
16. D. PISLA, et al., *Innovative parallel robot for lower limb rehabilitation,* Patent pending no. A00391/27.06.2019.
17. B. GHERMAN, I. BIRLESCU, P. TUCAN, C. VAIDA, A. PISLA, D. PISLA, *Modelling and simulation of a robotic system for lower limb rehabilitation*, ASME 2018 International Design Engineering Technical Conferences and Computers and Information in Engineering Conference, Quebec, Paper no. DETC2018-85872, 2018.
18. B. GHERMAN, I. BIRLESCU, F. PUSKAS, A. PISLA, G. CARBONE, P. TUCAN, A. BANICA, D. PISLA, *A kinematic characterization of a parallel robotic system for lower limb rehabilitation*, EuCoMeS 2018, Mechanisms and Machine Science, **59**, pp. 27-34, 2019.
19. V. CHIROIU, L. MUNTEANU, C. RUGINĂ, *On the control of a cooperatively robotic system by using hybrid logic algorithms*, Proceedings of the Romanian Academy, Series A, **19**, *4*, pp. 589-596, 2018.
20. L. MOLDOVAN, A. GLIGOR, H.-S. GRIF, F. MOLDOVAN, D*ynamic numerical simulation of the 6-PGK parallel robot manipulator*, Proceedings of the Romanian Academy, Series A, **20**, *1*, pp. 67-75, 2019.
21. R. JHA, D. CHABLAT, L. BARON, F. ROUILLIER, G. MOROZ, *Workspace, joint space and singularities of a family of delta-like robot*, Mechanism and Machine Theory, **127**, pp. 73-95, 2019.
22. D. COX, J. LITTLE, D. O'SHEA, *Ideals, varieties, and algorithms: An introduction to computational algebraic geometry and commutative algebra*, Springer-Verlag, New York, 2007.

Received April 17, 2019